

MIT Open Access Articles

Hand-held Schlieren Photography with Light Field probes

The MIT Faculty has made this article openly available. **Please share** how this access benefits you. Your story matters.

Citation: Wetzstein, Gordon, Ramesh Raskar, and Wolfgang Heidrich. "Hand-held Schlieren Photography with Light Field probes." In 2011 IEEE International Conference on Computational Photography (ICCP), 1-8.

As Published: <http://dx.doi.org/10.1109/ICCPHOT.2011.5753123>

Publisher: Institute of Electrical and Electronics Engineers (IEEE)

Persistent URL: <http://hdl.handle.net/1721.1/79911>

Version: Author's final manuscript: final author's manuscript post peer review, without publisher's formatting or copy editing

Terms of use: Creative Commons Attribution-Noncommercial-Share Alike 3.0



Hand-Held Schlieren Photography with Light Field Probes

Gordon Wetzstein^{1,2}

Ramesh Raskar²

Wolfgang Heidrich¹

¹The University of British Columbia

²MIT Media Lab

Abstract

We introduce a new approach to capturing refraction in transparent media, which we call *Light Field Background Oriented Schlieren Photography (LFBOS)*. By optically coding the locations and directions of light rays emerging from a light field probe, we can capture changes of the refractive index field between the probe and a camera or an observer. Rather than using complicated and expensive optical setups as in traditional Schlieren photography we employ commodity hardware; our prototype consists of a camera and a lenslet array. By carefully encoding the color and intensity variations of a 4D probe instead of a diffuse 2D background, we avoid expensive computational processing of the captured data, which is necessary for *Background Oriented Schlieren imaging (BOS)*. We analyze the benefits and limitations of our approach and discuss application scenarios.

1. Introduction

The acquisition of refractive phenomena caused by natural objects has been of great interest to the computer graphics and vision community. Joint optical light modulation and computational processing can be used to reconstruct refractive solids, fluids, and gas flows [15], render complex objects with synthetic backgrounds [34], or validate flow simulations with measured data. Unfortunately, standard optical systems are not capable of recording non-linear trajectories that photons travel along in inhomogeneous media. In this paper, we present a new approach to revealing refractive phenomena by coding the colors and intensities of a light field probe. As illustrated in Figure 1, the probe is positioned behind an object of interest and the object and probe are photographed by a camera. Due to refractions caused by the medium, apparent colors and intensities of the probe change with the physical properties of the medium, thereby revealing them to the camera or a human observer.

The idea of optically transforming otherwise invisible physical quantities into observed colors and changes in intensity is not new. In fact it occurs in nature in the form of caustics. These types of phenomena are generally referred

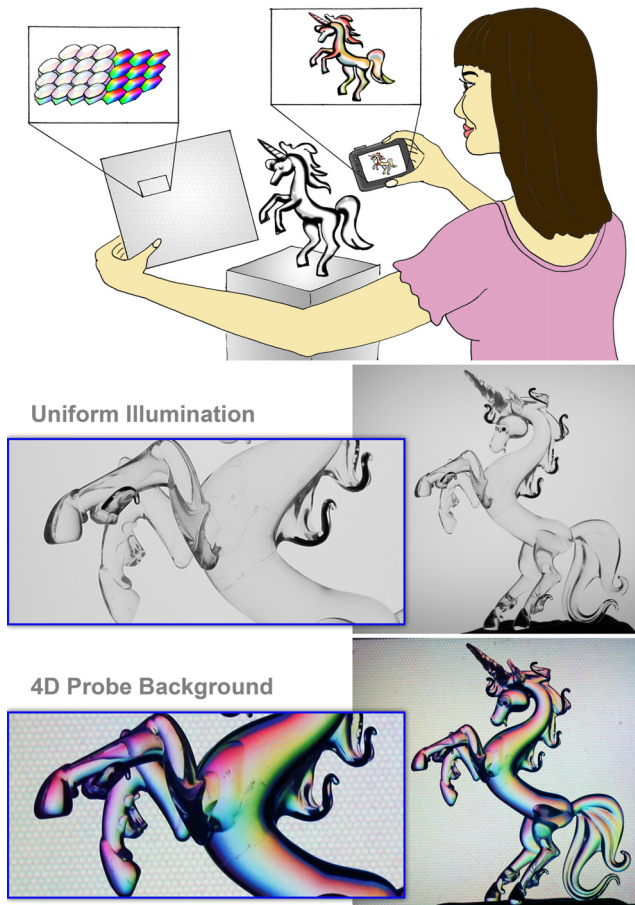


Figure 1. Light field probes —when included into the background of a scene— allow otherwise invisible optical properties to be photographed. In this example, the probe contains a classic Rainbow Schlieren filter that codes the angles and magnitudes of complex refractive events in hue and saturation.

to as Shadowgraphs and reveal only limited information of the underlying physical processes [31]. More sophisticated techniques to visualizing and photographing gas and fluid flows, refractive solids, and shock waves were developed in the 1940s [30]. Some of the phenomena that were depicted for the first time include the shock waves created by jets breaking the sound barrier and bullets flying through the air, or the heat emerging from our bodies. As illustrated in Fig-

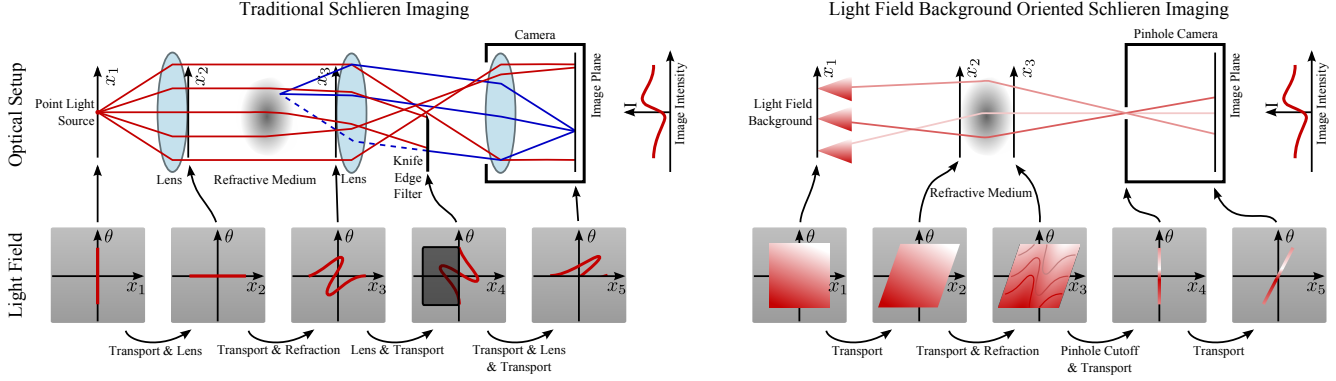


Figure 2. Illustration of optical setups and light field propagation for traditional Schlieren imaging (left) and Light Field Background Oriented Schlieren photography (right). Optical paths for forward light propagation to the camera are red, whereas backward propagation paths from a camera pixel are blue. Please note that the 4D light field probe illustrated on the right only codes the two angular dimensions in this case.

ure 2 (left, red lines), traditional Schlieren setups require collimated illumination, which is then optically disturbed by changes in the refractive index of a medium. A lens deflects all light rays so that the 'regular' rays, those that were not refracted, intersect that plane at one specific point, usually the center. The 'irregular' or refracted rays intersect the plane at different points, which are determined by the angle and magnitude of the refraction. Optical filters such as knife edges or color wheels can be mounted in that plane to encode these properties in color or intensity. Further light propagation optically transforms the rays back to their 'normal' distribution and an image can be recorded with a camera. Each pixel on the sensor is focused on a specific point in the refractive medium (Figure 2, left, blue lines), which allows an image to be formed along with intensity or color changes caused by the refraction. Although recent improvements have made traditional Schlieren setups more practical [32], fundamentally, these approaches require precise calibration and high-quality optical elements that are at least as big as the observed objects. Therefore, these systems are usually bulky, expensive, and mostly constrained to laboratory environments.

With the increase of computational power, Background Oriented Schlieren imaging (BOS) [8] was invented to overcome the difficulties of traditional Schlieren photography. In BOS, a digital camera observes a planar high-frequency background through a refractive medium. Optical flow algorithms are used to compute a per-pixel deflection vector with respect to an undistorted reference background. This type of optical flow estimation requires the background to be diffuse or photo-consistent.

Light Field Background Oriented Schlieren photography (LFBOS) also employs a background probe, but rather than coding only two dimensions, we can encode up to four dimensions of the light field: spatial and angular variation. Figure 3 shows a comparison of the most important

characteristics of LFBOS compared with BOS and traditional Schlieren imaging. The asterisk indicates that although BOS backgrounds have a high spatial resolution and no angular variation, these patterns are usually placed at a large distance to the object so that they effectively become angular-only probes. This increases the size of the setup and often results in focus discrepancies between background and object. Our probes have a small form factor and do not suffer from focus mismatches.

	Trad. Schlieren	BOS	LFBOS
Coded Dimensions	2D	2D	4D
Setup Complexity	moderate-difficult	easy	easy
Angular Resolution	very high	N/A*	high
Spatial Resolution	N/A	very high*	moderate
Processing	low	very high	low
Cost	high	low	low
Form Factor	usually bulky	usually bulky*	small

Figure 3. Overview of Light Field Background Oriented Schlieren photography compared to traditional and Background Oriented Schlieren photography (* see text).

We demonstrate successful acquisitions of refractions in fluids and solids, however, the employed off-the-shelf hardware in our current prototypes is a limiting factor for their precision. Slight angular deflections in gases and shock waves are therefore difficult to capture. We make the following contributions:

- introduction of the concept of computational light field probes for recording and processing new kinds of visual information with off-the-shelf cameras;
- presentation of a new type of Background Oriented Schlieren imaging that is portable, alleviates the problem of focus discrepancies, and allows spatial and angular information to be coded.

Furthermore, we discuss application specific optimality criteria for designing light field probes, compare our work with previous approaches, point out limitations of our technique, and present a variety of application scenarios.

2. Related Work

Fluid Imaging is a wide and active area of research. Generally, approaches to measure fluid flows can be categorized into optical and non-optical methods. Non-optical methods make velocity fields observable by inducing particles, dye, or smoke; alternatively, the surface shear, pressure forces, or thermal reactions can be measured on contact surfaces that are coated with special chemicals. Optical fluid imaging methods include Schlieren photography and holographic interferometry, which are based on ray and wave models of light, respectively. LFBOS is an optical fluid imaging approach that uses a ray-based light model. An extensive overview of fluid imaging techniques can be found in the book by Merzkirch [22].

Traditional Schlieren Photography is a non-intrusive imaging method for dynamically changing refractive index fields. These techniques have been developed in the fluid imaging community over the past century, with substantial improvements in the 1940s by Schardin and his colleagues [30]. A good overview of different optical setups and the historic evolution of Schlieren and Shadowgraph imaging can be found in the book by Settles [31]. Unfortunately, the optical setups require precisely registered high-quality mirrors and lenses, which are expensive, usually bulky, and difficult to calibrate. Our approach uses an inexpensive light field probe that encodes refractions in variation of color and intensity; our current prototype implements this concept with a lenslet array and a transparency.

In the last decade, **Background Oriented Schlieren Imaging (BOS)** [8, 29, 21, 9, 11] has been developed. Here, complicated optical apparatuses are replaced by optical flow calculations; an evaluation of these algorithms for BOS can be found in Atcheson et al. [2]. Because of the simplified setup, BOS makes it feasible to set up multi-view Schlieren imaging systems that can be used for tomographic reconstruction of 3D distortion volumes [3]. Just like BOS, our approach uses a background probe, which is observed through the refractive medium. However, rather than estimating the distortion of a diffuse background with computationally expensive optical flow estimators, we optically encode spatial and angular light variation with our light field probe. The computational part of LFBOS is a pre-processing step that determines the colors and layout of the probe.

Light Field Displays have been used for a variety of different applications such as presenting 3D image content [27, 19], consistent illumination in augmented reality [7], passive 6D displays that are responsive to the environment

illumination [10], new types of barcodes [24], and measuring the refractive errors of the human eye [28]. The work that is probably closest to ours is the light field microscope [20]. This device has an integrated light field illumination mechanism that can produce exotic lighting effects on the specimen. The light field microscope uses 4D illumination for reflective, microscopic objects; LFBOS on the other hand optically codes the background behind a transparent medium to visualize and quantify refractions caused by solids or liquids in macroscopic environments.

Unlike most techniques in **phase-contrast microscopy** [26], such as Zernike phase contrast and differential interference contrast (DIC), LFBOS does not require coherent illumination.

In **Computer Graphics and Vision**, scanning static transparent objects [5, 23, 25, 18, 33] as well as dynamic transparent media, such as liquids [14], flames [12, 16], and gas flows [3], has been of much interest in recent years. We do not aim at reconstructing three-dimensional objects or refractive index fields; although using LFBOS probes for these applications is an interesting avenue of future work.

3. Theory

3.1. Image Formation

The propagation of light in inhomogeneous refractive media is governed by the ray equation of geometric optics [6]:

$$\frac{\partial}{\partial s} \left(n \frac{\partial \mathbf{x}}{\partial s} \right) = \nabla n, \quad (1)$$

where \mathbf{x} is the position of a photon on a trajectory in space, ∂s is the differential path length along the trajectory, and n is the (spatially varying) refractive index field. The wavelength dependency of n is disregarded in this model. Equation 1 can be formulated as a coupled system of first-order ODEs [17, 3]:

$$n \frac{\partial \mathbf{x}}{\partial s} = \mathbf{d}, \quad \frac{\partial \mathbf{d}}{\partial s} = \nabla n, \quad (2)$$

with \mathbf{d} being the local direction of propagation. Integrating Equation 2 leads to an expression for the global directional deformation within a refractive object [3]:

$$\mathbf{d}^{out} = \mathbf{d}^{in} + \int_c \nabla n ds. \quad (3)$$

In our setup, the refractive index field is observed against a known light field background, as shown in Figure 2 (right). In order to understand the distortion of this known 4D probe, Equation 2 can be solved numerically, for instance with forward Euler schemes [17]. However, in our case it is more intuitive to trace the light field on the sensor plane back to the probe. Considering a pinhole camera, as

shown in Figure 2 (right), the light field probe $l(x, y, \theta, \phi)$ is sampled in the following way:

$$i(\mathbf{x}_p) = l\left(\varsigma(\mathbf{x}_p, \mathbf{d}_p), \varphi\left(\mathbf{d}_p + \int_c \nabla n ds\right)\right). \quad (4)$$

Here, i is the sensor image and \mathbf{d}_p the normalized direction from a pixel $\mathbf{x}_p = (x_p^x, x_p^y)$ to the camera pinhole. The function $\varphi(\mathbf{d})$ maps a direction $\mathbf{d} = (d^x, d^y, d^z)$ to the angular parameterization of the light field, i.e. $\varphi_{\theta, \phi}(\mathbf{d}) = (\tan^{-1}(d^x/d^z), \tan^{-1}(d^y/d^z))$. The position and direction of a light ray incident on a pixel can be mapped to a position on the probe by the function ς ; this depends on the distances between camera and object, object and probe, and the ray displacement within the object. If the ray displacement is negligible, the refractive medium can be approximated as a thin element that causes a single refractive event, such as a thin lens. In our model we neglect intensity variations caused by the camera pinhole or the specific structure of the probe (e.g. lenslets).

Although pinhole cameras sample discrete rays of the refracted light field, in practice cameras usually have a finite aperture implying that each pixel integrates over a small range of light field directions on the probe. We assume that the distance between the light field probe and the camera is large compared to the size of the aperture and that the distance between the probe and the refractive object is small, which yields a good approximation of a pinhole camera.

3.2. Designing Light Field Probes

The goal of LFBOS is to encode the directions and locations of a 4D probe with color and intensity variations so that the former parameters can be inferred from the colors in a photograph. The immediate question that arises is how one can design a light field probe that encodes positions and directions in a meaningful way. To answer this question, we need to consider a number of application-specific parameters that are discussed in the following.

Although a pinhole camera is a reasonable approximation under the above mentioned assumptions, finite pixel sizes and small apertures along with strong distortions of the wavefront caused by refraction often amplify the integration area of each camera pixel in the space of the light field probe. In order to compensate for this effect, the distribution of *color tones and intensities* in the probe should be *smooth* in the 4D spatio-directional domain. This also implies graceful degradation of the captured colors in case the pinhole assumption breaks down.

If the absorption of light within the refractive medium is not negligible, the color distributions should ideally be independent of intensity changes. This can, for instance, be implemented by encoding the desired parameters only in hue and saturation, i.e. constant values in HSV color

space. Doing so also ensures resilience to vignetting and other possible intensity changes caused by the lenslets of the probe.

Positions and directions of a background light field can either be encoded in the *absolute* 4D reference frame of the probe or *relative* to a fixed camera position. This is not necessary for orthographic cameras, but to *compensate for the perspective* of a non-orthographic camera.

4. Prototype and Experiments

4.1. Prototypes

We have implemented prototypes of our light field probes using both lenticular sheets with cylindrical lenses and lenslet arrays with hexagonal grids of spherical lenses. These make a tradeoff between spatial and angular resolution. The specific lenslet arrays we have used in our experiments along with their spatial and angular resolution and fields-of-view are listed in Table 1. Alternative implementations of 4D probes include holograms (e.g. www.zebraimaging.com) or dynamic parallax barrier displays (e.g. [19]); these allow for probes with a very high spatial and angular resolution.

Lenslet Type	f [in]	d [in]	fov [°]	Angular Resolution [°]		
				600 dpi	2038 dpi	5080 dpi
MicroLens Animation 10	0.11	0.1	48	0.80	0.24	0.09
MicroLens 3D 20	0.10	0.05	29	0.97	0.28	0.11
FresnelTech Hexagonal 300	0.12	0.09	42	0.77	0.23	0.09
FresnelTech Hexagonal 310	1.00	0.94	51	0.09	0.03	0.01

Table 1. Technical specifications of the lenslet arrays used in our experiments.

The lenslet arrays are mounted on a light box that provides a uniform background illumination. We print the probe codes at a resolution of 1200 dpi on transparencies that are manually aligned with the lenslet arrays before mounting them on the light box. For an increased contrast, multiple transparencies can be stacked. Care must be taken with the non-linear color transformations between specified digital images, the printer gamut, and the color gamut of the camera. We define our patterns within the device-specific CMYK color gamut of the employed printer (RGB and CMYK ICC profiles of printers are usually available from the manufacturer), then print them with device-internal color mappings disabled, and record camera images in sRGB space. This process allows us to transform the captured photographs to any desired color space as a post-processing step.

4.2. Angular Filtering

Figures 4, 5, and 6 demonstrate a variety of different intensity and color filters encoded in the probes; these reveal angular variation caused by refraction. For the experiments discussed below, the encoded light field is pre-distorted to

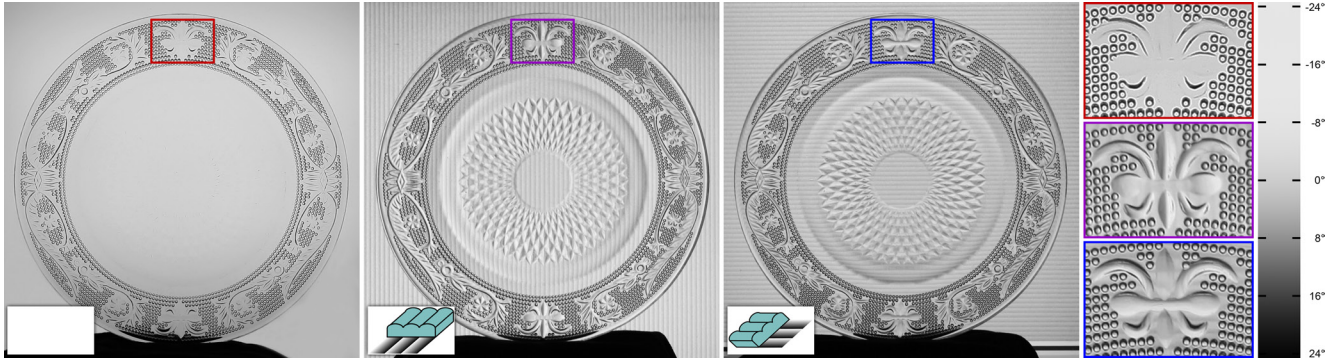


Figure 4. A plate in front of a uniform background (left), and a light field probe that encodes directional variation caused by refraction with a horizontal (center left) and a vertical (center right) intensity gradient. The magnifications (right) and the structure on the plate show how otherwise invisible information is revealed with our probes. The color bar, mapping colors to magnitudes of refraction, is computed from the field of view of the lenticulars and a calibration gradient that is cropped from the photographs.

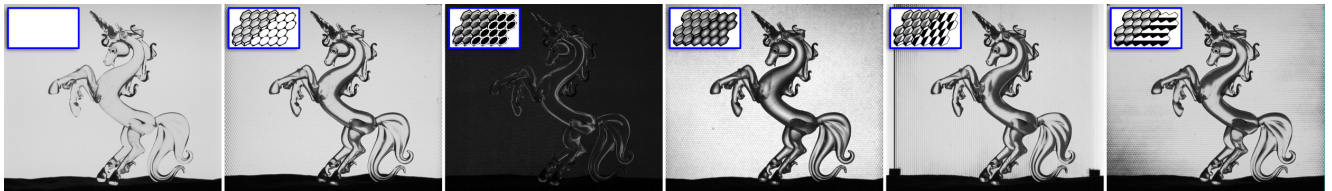


Figure 5. A variety of directional filters can be encoded in our probes. From left: uniform background, annular bright field, annular dark field, circular intensity gradient, horizontal cutoff, and vertical cutoff.



Figure 6. The classic Rainbow Schlieren filter encoded in our light field probe can visualize magnitudes and angles of refractions in complex media such as this mix of clear corn syrup and water.

account for the perspective of the camera. An undistorted view of the probe from the camera position therefore shows the center of a specific angular probe code.

Intensity Gradients correspond to knife edge filters in traditional Schlieren imaging. These filters usually sacrifice half of the background illumination by coding undistorted rays in gray; the magnitudes of light deflection in a particular direction are coded in increasing or decreasing intensity. An example of one-dimensional gradients is shown in Figure 4. Here, lenticular sheets are used as probes where the gradient under each cylindrical lens is equal except for a varying lens-to-lens pitch that corrects for the perspective of the camera. As an alternative to 1D gradients, a circular gradient under each circular lens of a hexagonal lenslet array can encode the magnitudes of deflected rays as seen in Figure 5 (center right).

Annular Bright Field and Dark Field Filters are inspired by microscopy [26, 20], where similar illumination patterns can be used to illuminate reflective or refractive specimen. The annular bright field probe code is a uniform circular pattern with a small black outline that does not effect undeflected rays or those that underwent only small amounts of refraction. Strong refractions, as seen on the object boundaries of the unicorn in Figure 5 (second from left), are completely blocked. The inverse of the annular bright field is the annular dark field, which only allows rays with strong refractions to reach the camera (see Figure 5, third from left).

Directional Cutoffs can be used to completely block ray deflections into a certain direction. An example of this filter type can be seen in the vertical-only and horizontal-only cutoff shown in Figure 5 (the two rightmost images).

Color Filters are popular in traditional Schlieren setups. Usually, these approaches are called Rainbow Schlieren [13] and allow the magnitude and the angle of ray deflection to be encoded in different color gradients. The HSV color wheel is a popular choice for the filter. Undelected rays are coded in white, whereas the deflection angle is coded in hue and the magnitude in saturation of the color wheel. Examples of these filters are shown in Figures 1 and 6.

4.3. Spatio-Angular Filtering

So far, we have only considered probes with purely angular filters. Light field probes, however, allow us to additionally encode the spatial locations on the probe. Following the probe design criteria discussed in Section 3.2, we experimented with light field probes that encode the 2D angular domain and one of the spatial dimensions in three color primary gradients.

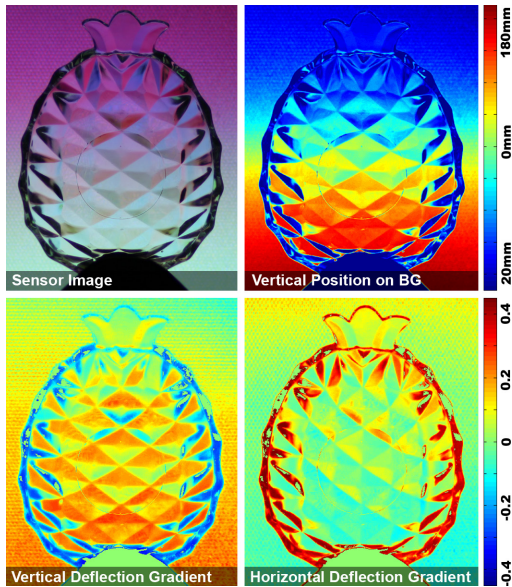


Figure 7. A refractive object in front of a light field probe (upper left) that encodes vertical ray displacement (upper right) as well as vertical and horizontal ray deflection. The latter two quantities can be used to compute the gradient of the refractive index field as shown in the lower row.

The scene in Figure 7 (upper left) is photographed in front of a probe that codes horizontal and vertical angular ray deflections in red and blue color gradients, respectively, and the vertical position on the probe in a green gradient. The absolute color values are defined within the color gamut of the printer.

In addition to the spatio-angular color codes, we include fiducial markers on the probe (cropped from the image) that allow us to estimate the extrinsic camera parameters from a single photograph. Given the intrinsic and extrinsic cam-

era parameters, we can easily compute the undistorted angle and position of each light ray emerging from a camera pixel on the probe background. The light field probe is registered with the markers, so that each ray that is emitted by the probe uniquely encodes its angle and location in colors.

Therefore, by taking a photograph of the probe without any refractive media in the optical path the expected ray locations and angles on the probe match the encoded colors. However, if variations in the refractive index field in between probe and camera cause changes in ray trajectories, these changes in ray angle and displacement are directly observable in the recorded colors as seen in Figure 7. By applying Equations 3 and 4 to the observed and expected light rays, we can compute a per-pixel refractive index gradient (Figure 7, lower row) and vertical ray displacement (Figure 7, upper right). Reconstructing refractive index fields of gases, fluid flows, and the shape of transparent solids using these quantities is an interesting avenue of future work.

5. Comparison to BOS

Background Oriented Schlieren setups usually require a high-frequency background to be located at a large distance to the object. In this way, the per-pixel displacement vectors estimated by optical flow are proportional to the angular ray deflections, which is related to the refractive index gradient (Eq. 3). The form factor of these setups is therefore usually large. Furthermore, the camera needs to be focused on the background pattern so that its distortion can be tracked by the optical flow algorithm. The total amount of light in BOS setups is often limited, which is why cameras typically need to use a large aperture for capture. Unfortunately, this places the object of interest out-of-focus as seen in Figure 8 (upper left).

Strong refractions, for instance caused by fluids or solids, often lead to extreme distortions of the background pattern. These distortions may prevent a reliable optical flow estimation as shown in Figure 8 (upper right). Although an optical flow algorithm for refractive objects has been proposed [1], this requires many frames of a video sequence to be analyzed and is not practical for dynamic media such as fluids.

In comparison, our approach requires only a single image and the light field background can be placed at close proximity to the object, which alleviates the focus mismatch problem (Figure 8, lower left). Furthermore, if the light field probe encodes smooth gradients, as discussed in Section 3.2, even a defocused refractive object will reveal the mean of colors and intensities in the integration manifold of the 4D probe space to a camera pixel (Figure 8, lower right).

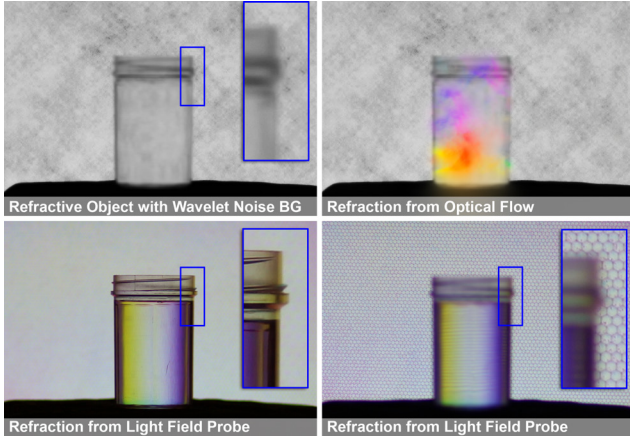


Figure 8. Light Field Background Oriented Schlieren photography compared to a failure case of Background Oriented Schlieren imaging. Optical flow algorithms in BOS require the background to be focused, which places the object out-of-focus (upper left). In this case, the refractions are so strong that they blur out the background pattern and therefore prevent a reliable optical flow estimation (upper right). LFBOS works for in-focus (lower left) and out-of-focus settings (lower right).

6. Limitations

As in most Schlieren approaches, the size of the refractive volume is limited by the size of the employed optical elements, in our case the light field probe. An exception are traditional Schlieren setups that use the sun or other distant point lights as the source of the required collimated illumination and Natural-Background Oriented Schlieren techniques [11], which also work outdoors. Currently, both phase and amplitude of the medium caused by refraction and absorption, respectively, are captured. For faithful reconstruction of objects with non-negligible absorption, these effects need to be separated [4]. Furthermore, we assume that there is no scattering or emission within the medium and neglect any wavelength-dependency of refractive events.

One of the major limitations of our prototypes is the limited resolution and color gamut of the printer. All of the transparencies in our experiments were printed with off-the-shelf inkjet printers, usually with 1200dpi. Alternative processes are light valve technology, which exposes digital images with a high resolution, contrast, and color gamut onto film (www.bowhaus.com), or professional offset printing.

All of our current prototypes are implemented with lenslet arrays or lenticulars, which trade spatial and angular resolution. A very high spatial and angular resolution can be achieved with alternative technologies, such as holograms (www.zebraimaging.com) or dynamic parallax barrier displays [19]. When the camera is focused on a lenslet-based probe, the space between individual lenses usually appears darker. This problem could also be overcome with

alternative probe implementations.

As the fields-of-view of the lenslets in our current prototypes are defined by the manufacturing process, refractions that exceed the field-of-view cannot be coded reliably. An example of such a failure case is shown in Figure 9. The same problem often occurs in parallax-barrier or lenslet-based auto-stereoscopic displays. For our application, the lenslets for a specific experiment should be chosen in accordance with the expected amount of refraction. While the lenslets in our experiments (Table 1) are successful in capturing moderate to strong refractive events caused by liquids and solids, the precision and sensitivity of our current probes, which are made from off-the-shelf hardware, is currently too low to faithfully acquire the slight angular deflections within gas flows or shock waves.



Figure 9. Failure case: the field-of-view of the lenslet array is too narrow to properly encode the strong refractions near the sides of the glass. To overcome this, the lenslets should be chosen according to the amount of refraction in the scene.

7. Discussion and Future Work

In summary, we have presented a new approach to capturing refractive phenomena using light field probes. Our approach presents a portable and inexpensive alternative to traditional and Background Oriented Schlieren imaging; it works well with strong refractions, which is often not the case for BOS, and also alleviates the focus mismatch between background and objects of interest. Inspired by Schlieren imaging and microscopy, we have shown how a variety of different filters for visualizing refractive events can be encoded in our light field probes and recorded with off-the-shelf cameras.

In the future, we would like to experiment with alternative technologies for 4D probes, which allow for a high spatial and angular resolution. We would also like to explore smaller probe designs using LED or OLED-based backlights instead of light boxes. Furthermore, we will investigate more sophisticated color coding schemes for the 4D light field probe space and reconstruct 3D refractive index fields from fluid and gas flows as well as surfaces of refractive solids.

In addition to measuring refraction, 4D light field probes could be useful for a variety of other applications including

BTDF and BRDF estimation, de-scattering, and separating local and global illumination.

Acknowledgements

We thank Roarke Horstmeyer for discussions and Matt Hirsch for proofreading the manuscript. Gordon Wetzstein was supported by a UBC 4 year fellowship. This project was in part supported by the GRANT NCE.

References

- [1] S. Agarwal, S. P. Mallick, D. Kriegman, and S. Belongie. On Refractive Optical Flow. In *Proc. ECCV*, pages 483–494, 2004. 6
- [2] B. Atcheson, W. Heidrich, and I. Ihrke. An Evaluation of Optical Flow Algorithms for Background Oriented Schlieren Imaging. *Experiments in Fluids*, 46(3):467–476, 2009. 3
- [3] B. Atcheson, I. Ihrke, W. Heidrich, A. Tevs, D. Bradley, M. Magnor, and H.-P. Seidel. Time-resolved 3D Capture of Non-stationary Gas Flows. *ACM Trans. Graph. (Proc. SIGGRAPH Asia)*, 27(5):132, 2008. 3
- [4] E. D. Barone-Nugent, A. Barty, and K. A. Nugent. Quantitative Phase-Amplitude Microscopy I: Optical Microscopy. *Journal of Microscopy*, 206(3):194–203, 2002. 7
- [5] M. Ben-Ezra and S. K. Nayar. What Does Motion Reveal About Transparency? In *Proc. ICCV*, pages 1025–1032, 2003. 3
- [6] M. Born and E. Wolf. *Principles of Optics*. Cambridge University Press, 7 edition, 1999. 3
- [7] O. Cossairt, S. K. Nayar, and R. Ramamoorthi. Light Field Transfer: Global Illumination Between Real and Synthetic Objects. *ACM Trans. Graph. (Proc. SIGGRAPH)*, 27(3):57, 2008. 3
- [8] S. Dalziel, G. Hughes, and B. Sutherland. Whole-Field Density Measurements by Synthetic Schlieren. *Experiments in Fluids*, 28(4):322–335, 2000. 2, 3
- [9] G. Elsinga, B. Oudheusden, F. Scarano, and D. Watt. Assessment and Application of Quantitative Schlieren Methods: Calibrated Color Schlieren and Background Oriented Schlieren. *Experiments in Fluids*, 36(2):309–325, 2004. 3
- [10] M. Fuchs, R. Raskar, H.-P. Seidel, and H. P. A. Lensch. Towards Passive 6D Reflectance Field Displays. *ACM Trans. Graph. (Proc. SIGGRAPH)*, 27(3):58, 2008. 3
- [11] M. J. Hargather and G. S. Settles. Natural-Background-Oriented Schlieren Imaging. *Experiments in Fluids*, 48(1):59–68, 2009. 3, 7
- [12] S. W. Hasinoff and K. N. Kutulakos. Photo-Consistent Reconstruction of Semitransparent Scenes by Density-Sheet Decomposition. *Trans. PAMI*, 29(5):870–885, 2007. 3
- [13] W. L. Howes. Rainbow Schlieren and its Applications. *Applied Optics*, 23(4):2449–2460, 1984. 6
- [14] I. Ihrke, B. Goldluecke, and M. Magnor. Reconstructing the Geometry of Flowing Water. In *Proc. ICCV*, pages 1055–1060, 2005. 3
- [15] I. Ihrke, K. N. Kutulakos, H. P. A. Lensch, M. Magnor, and W. Heidrich. Transparent and Specular Object Reconstruction. *Computer Graphics Forum*, 2010, to appear. 1
- [16] I. Ihrke and M. Magnor. Image-Based Tomographic Reconstruction of Flames. In *Proc. SCA*, pages 367–375, 2004. 3
- [17] I. Ihrke, G. Ziegler, A. Tevs, C. Theobalt, M. Magnor, and H.-P. Seidel. Eikonal Rendering: Efficient Light Transport in Refractive Objects. *ACM Trans. Graph. (Proc. SIGGRAPH)*, 26(3):59, 2007. 3
- [18] K. N. Kutulakos and E. Steger. A Theory of Refractive and Specular 3D Shape by Light-Path Triangulation. In *Proc. ICCV*, pages 1448–1455, 2005. 3
- [19] D. Lanman, M. Hirsch, Y. Kim, and R. Raskar. Content-Adaptive Parallax Barriers for Automultiscopic 3D Display. *ACM Trans. Graph. (Proc. SIGGRAPH Asia)*, 29(5), 2010. 3, 4, 7
- [20] M. Levoy, Z. Zhang, and I. McDowall. Recording and Controlling the 4D Light Field in a Microscope. *Journal of Microscopy*, 235(2):144–162, 2009. 3, 5
- [21] G. Meier. Computerized Background-Oriented Schlieren. *Experiments in Fluids*, 33(1):181–187, 2002. 3
- [22] W. Merzkirch. *Flow Visualization*. Academic Press, 1987. 3
- [23] D. Miyazaki and K. Ikeuchi. Inverse Polarization Raytracing: Estimating Surface Shapes of Transparent Objects. In *Proc. CVPR*, pages 910–917, 2005. 3
- [24] A. Mohan, G. Woo, S. Hiura, Q. Smithwick, and R. Raskar. Bokode: Imperceptible Visual Tags for Camera Based Interaction from a Distance. *ACM Trans. Graph. (Proc. SIGGRAPH)*, 28(3):98, 2009. 3
- [25] N. J. W. Morris and K. N. Kutulakos. Dynamic Refraction Stereo. In *Proc. ICCV*, pages 1573–1580, 2005. 3
- [26] D. B. Murphy. *Fundamentals of Light Microscopy and Electronic Imaging*. Wiley-Liss, 2001. 3, 5
- [27] F. Okano, J. Arai, H. Hoshino, and I. Yuyama. Three-Dimensional Video System Based on Integral Photography. *Optical Engineering*, 38(6):1072–1077, 1999. 3
- [28] V. F. Pamplona, A. Mohan, M. M. Oliveira, and R. Raskar. NETRA: Interactive Display for Estimating Refractive Errors and Focal Range. *ACM Trans. Graph. (Proc. SIGGRAPH)*, 29(4):77, 2010. 3
- [29] H. Richard and M. Raffel. Principle and Applications of the Background Oriented Schlieren (BOS) Method. *Measurement Science and Technology*, 12(9):1576–1585, 2001. 3
- [30] H. Schardin. Die Schlierenverfahren und ihre Anwendungen. *Ergebnisse der Exakten Naturwissenschaften. English translation available as NASA TT F-12731, April 1970 (N70-25586)*, 20:303–439, 1942. 1, 3
- [31] G. S. Settles. *Schlieren and Shadowgraph Techniques*. Cambridge University Press, 2001. 1, 3
- [32] G. S. Settles. Important Developments in Schlieren and Shadowgraph Visualization during the Last Decade. In *Proc. Int. Symp. on Flow Vis.*, page 267, 2010. 2
- [33] B. Trifonov, D. Bradley, and W. Heidrich. Tomographic Reconstruction of Transparent Objects. In *Proc. EGSR*, pages 51–60, 2006. 3
- [34] D. E. Zongker, D. M. Werner, B. Curless, and D. H. Salesin. Environment Matting and Compositing. In *ACM Trans. Graph. (Proc. SIGGRAPH)*, pages 205–214, 1999. 1